

A self-consistent approach to the one-dimensional chain models for the ferro- and antiferro-magnetism of nanotubes

Zhaosen Liu^a, Hou Ian^b

^aDepartment of Applied Physics, Nanjing University of Information Science and Technology, Nanjing 210044, China

^b Institute of Applied Physics and Materials Engineering, FST, University of Macau, Macau

Abstract

We employ a self-consistent simulation approach based on quantum theory to investigate the physical properties of a pair of ferromagnetic and antiferromagnetic nanotubes. It was observed that under the given conditions, no matter the external magnetic field was absent or applied along the easy longitudinal axis, the spins always ordered in that direction due to the special geometric shape of the tubes and the magnetic uniaxial anisotropy, so that the two sorts of nanosystems exhibit typical ferromagnetic and antiferromagnetic properties, which may find applications in modern technology, in strong contrast to the phenomena observed previously in nanoparticle [1], where an external magnetic field, applied parallel to the antiferromagnetically coupled spins, is able to turn the spins off their original direction to form symmetric pattern around the field direction. This peculiar feature enable us to build up one-dimensional chain models for the two sorts of nanosystems. Considering their fast computational speed and simplicity, these theoretical models were then utilized to investigate the finite size effects of the nanosystems, and perform further analysis for long tubes. Especially, our results obtained with the theoretical models and the numerical approach are exactly identical, verifying the correctness and applicability of the computational methodology.

Keywords: nanomagnet, quantum simulation model, computational algorithms, magnetic properties, nanotubes

Since the discovery of carbon nanotubes [2], the field of this kind of nanosystems, especially those exhibiting magnetic properties, have been attracting considerable attention due to their potential applications in modern technology as well as their significance in science [3, 4, 5, 6, 7]. For instance, high attention has been paid to the magnetic nanotubes based on the transition metals, such as CoPt, CoPd, FePt and FePd alloys owing to their potential applications in high-density magnetic recording media [8, 9, 10, 11, 12]. Now, one can find various new nanotubes based electronic and spintronic devices [13], multi-functional systems involving nanotubes for biotechnological applications [14].

So far, many techniques for fabricating magnetic nanotubes have been developed [15, 16, 17, 18, 19, 20]. Hematite α -Fe₂O₃ nanotubes can be produced for example by using a template method, which provides nanotubes with diameters between 100 nm and 200 nm, and a wall thickness less than 10 nm [16]; attachment of maghemite γ -Fe₂O₃ nanoparticles to the surface of carbon nanotubes via a modified sol-gel technique has also produced nano hybrid structures behaving as nanotubes [17].

Theoretically, electronic structures of ferromagnetic single-wall nanotubes were investigated by means of spin density functional theory [21]; continuous models for ferromagnetism [22], approaches based on Green functions [23], and simulation methods like Monte Carlo [24], have been

also employed to investigate the exotic magnetic properties and spin configurations of magnetic nanotubes.

In the present work, we first investigate the magnetic properties of a pair of ferromagnetic and antiferromagnetic nanocylinders, in which Heisenberg and uniaxial anisotropy along the central longitudinal z -axis co-exist, by means of a self-consistent approach based on quantum mean field theory. We find that the special geometric shape of the tube surfaces and the uniaxial anisotropy force the spins order in the easy z direction, so that the two sorts of nanosystems exhibit typical ferromagnetic and antiferromagnetic properties, which may find applications in modern technology, in strong contrast to the phenomena observed in antiferromagnetic nanoparticle [1], where an external magnetic field, parallel to the oppositely aligning spins, is able to turn the spins off their original direction to form symmetric pattern around the field direction. This peculiar feature of the nanosystems enables us to build up one-dimensional ferromagnetic and antiferromagnetic chain models for theoretical analysis. It turns out that the magnetizations, hysteresis curves, etc., generated by means of the numerical approach and the theoretical models are exactly identical, verifying our computational methodology once again.

1 Computational Model

Now, we consider a nano-cylinder, which is formed by rolling up a rectangular monolayer lattice consisting of $S=1$ spins sitting on the square lattice sites. The length of the nanotube is $\mathcal{L} = N_L a$ along the longitudinal central axis, where a is the lattice parameter, and there are N_R spins on every circle around the axis, i.e., the circumference of such a circle is $\mathcal{C} = N_R a$. Thus the coordinators of a spin on the nanotube wall are determined by

$$\begin{aligned} x_n &= \frac{N_R a}{2\pi} \cos\left(\frac{2\pi n}{N_R}\right) \\ y_n &= \frac{N_R a}{2\pi} \sin\left(\frac{2\pi n}{N_R}\right), \\ z_m &= ma, \end{aligned} \quad (1)$$

where $1 \leq n \leq N_R$, and $1 \leq m \leq N_L$.

To do Monte Carlo simulations for Ising-like nanocylinders, Masrouf et. al. only considered Heisenberg exchange interaction among the nearest neighboring spins with uniform strength, the uniaxial anisotropy along the longitudinal central axis, and the external magnetic field exerted in that direction [24]. Following Masrouf's work, the Hamiltonian for our single wall nanotubes thus can be expressed as

$$\mathcal{H} = -\frac{1}{2} \sum_{i,j \neq i} \mathcal{J}_{ij} \vec{S}_i \cdot \vec{S}_j - K_A \sum_i S_{iz}^2 - g_S \mu_B \sum_i S_{iz} B, \quad (2)$$

where $g_s=2$ is the Land factor, \mathcal{J}_{ij} and K_A represent the strengths of the exchange interaction among the neighboring spins and the uniaxial anisotropy assumed to be in the z -direction as well. In the above Hamiltonian, the spins are quantum operators instead of the classical vectors. Since $S=1$, the matrices of the three spin components in Cartesian coordinate system are given by

$$S_x = \frac{1}{2} \begin{pmatrix} 0 & \sqrt{2} & 0 \\ \sqrt{2} & 0 & \sqrt{2} \\ 0 & \sqrt{2} & 0 \end{pmatrix}, \quad S_y = \frac{1}{2i} \begin{pmatrix} 0 & \sqrt{2} & 0 \\ -\sqrt{2} & 0 & -\sqrt{2} \\ 0 & \sqrt{2} & 0 \end{pmatrix}, \quad S_z = \begin{pmatrix} 1 & 0 & 0 \\ 0 & 0 & 0 \\ 0 & 0 & -1 \end{pmatrix}, \quad (3)$$

respectively.

Since only the exchange interactions between the nearest spins are considered, a spin on the tube wall interacts only with its two nearest neighbors in the same line parallel to z axis with a strength of \mathcal{J}_1 , two nearest neighbors on the same circle around the central axis with a strength of \mathcal{J}_2 . When both \mathcal{J}_1 and \mathcal{J}_2 are positive, the nanotube is ferromagnetic, the spins tend to align in the same direction; while both \mathcal{J}_1 and \mathcal{J}_2 are negative, the nanotube is antiferromagnetic, every pair of neighboring spins attempt to order in the opposite directions.

This Hamiltonian given by Eq.(2) was first used to study the magnetic properties of the nanotubes numerically by means of the SCA approach [1, 25, 26]. In every simulation step, it was diagonalized so as to calculate the magnetic moment of the considered spin. All of our simulations were started here from a random magnetic configuration and a temperature well above the magnetic transition, then carried out stepwise down to very low temperatures with a temperature step $\Delta T < 0$. At any temperature, if the difference $|\langle \vec{S}_i \rangle - \langle \vec{S}_i \rangle|$ between two successive iterations for every spin is less than a very small given value τ_0 , convergency is considered to be reached [1, 25, 26].

2 Results Obtained Numerically with the SCA Approach

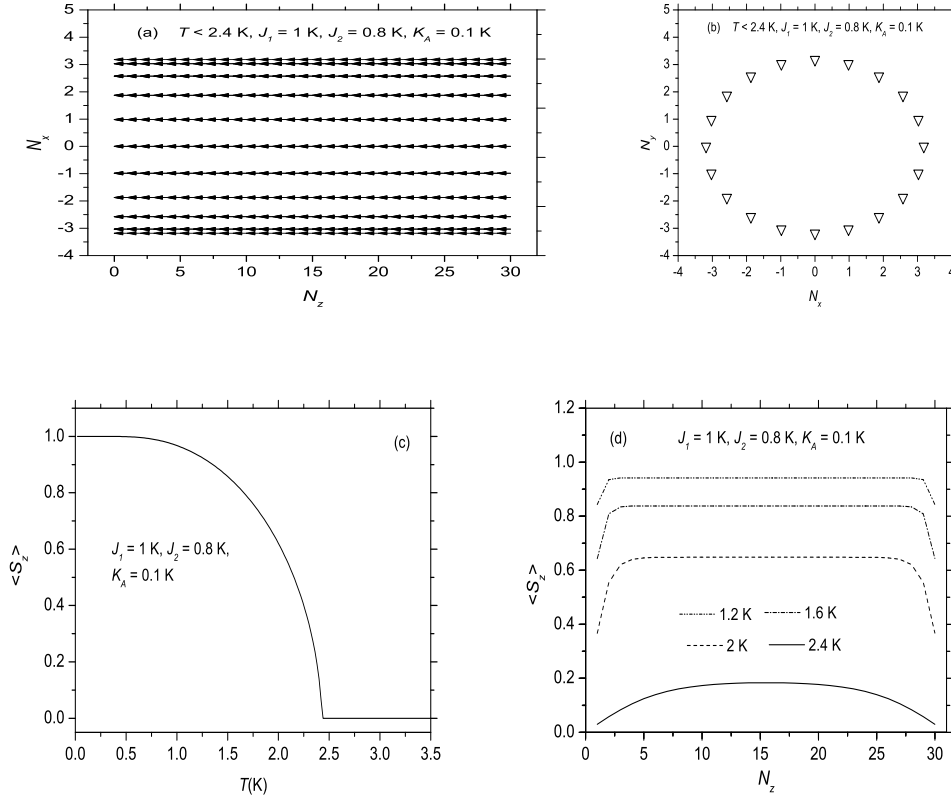


Figure 1. Simulated magnetic structures projected onto (a) $y = 0$, and (b) $z = 15a$ cross sections, respectively; calculated $\langle S_z \rangle$ (c) as function of temperature, and (d) as the function of z at different magnetic temperatures, for the ferromagnetic nanotube by means of the SCA approach in the absence of external magnetic field. Here $N_L = 30$.

Firstly, we performed simulations for a ferromagnetic nanotube with $N_L = 30$ and $N_R = 20$ by means of the SCA approach. To do this, Heisenberg exchange and uniaxial anisotropy strengths were assigned to $\mathcal{J}_1 = 1$ K, $\mathcal{J}_2 = 0.8$ K and $K_A = 0.1$ K, respectively. Fig.1(a,b) displays the magnetic structures projected onto the $y = 0$ and $z = 15a$ cross sections. As shown there, all spin order ferromagnetically antiparallel to the z -axis below Curie temperature $T_C \approx 2.44$ K. That is, in the magnetic phase, only $\langle S_z \rangle$ is nonzero, both $\langle S_x \rangle$ and $\langle S_y \rangle$ all vanish. As displayed in Fig.1(c), while temperature arises, $\langle S_z \rangle$ decreases gradually from the maximum value at very low temperatures to zero until T_C . Due to the finite length of the nanotube, we can find from Fig.1(d) that the spins near the two ends of the nanotube naturally have weaker magnitudes than those in the middle part at all recorded temperatures.

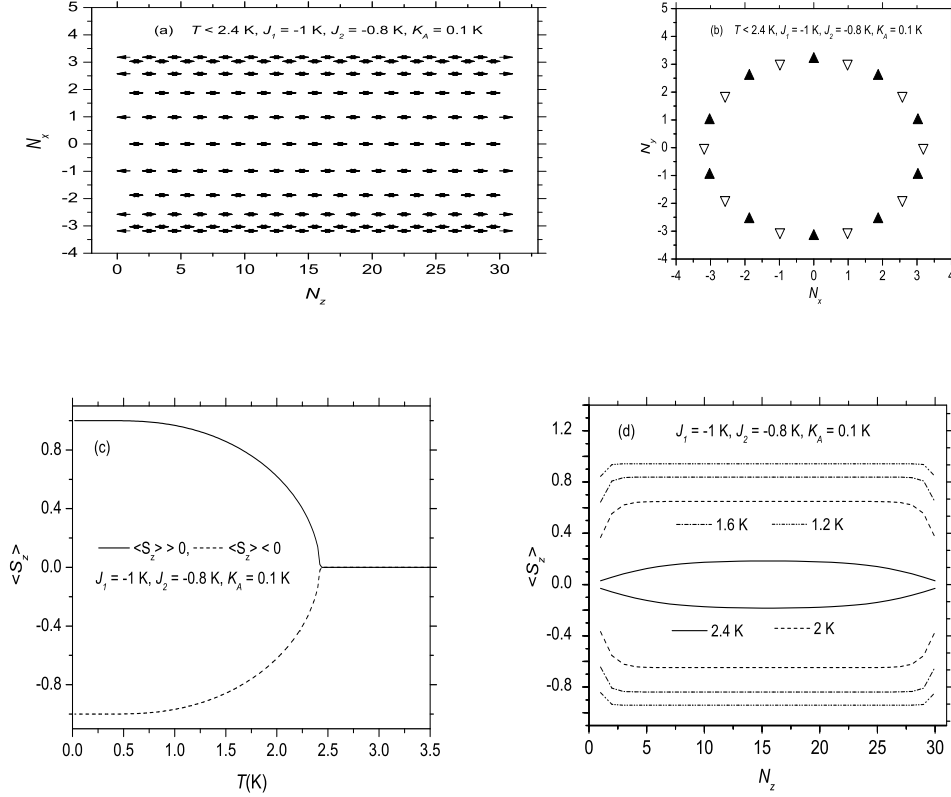


Figure 2. Simulated magnetic structures projected onto (a) $y = 0$, and (b) $z = 15a$ cross sections; calculated $\langle S_z \rangle$ (c) as the function of temperature, and (d) as the function of z at different temperatures, for the antiferromagnetic nanotube by means of the SCA approach in the absence of external magnetic field. Here $N_L = 30$.

For comparison with the results just obtained, we carried out simulations for an antiferromagnetic nanotube of the same size scale with the SCA approach by only changing the signs of the Heisenberg exchange constants, that is, now $\mathcal{J}_1 = -1$ K and $\mathcal{J}_2 = -0.8$ K. Fig.2(a,b) depict the magnetic configurations projected onto the $y = 0$ and $z = 15a$ cross sections. There we find that all spin order antiferromagnetically in the z -direction below Néel temperature $T_N \approx 2.44$ K. Once again, in the magnetic phase, only $\langle S_z \rangle$ is nonzero, both $\langle S_x \rangle$ and $\langle S_y \rangle$ all vanish. As temperature arises, the two opposite $\langle S_z \rangle$'s, depicted in Fig.2(c), attenuate gradually from the saturated value $S = 1$ at very low temperatures to zero at T_N . As N_z approaches to 1 or N_L from the middle region, $|\langle S_z \rangle|$ decreases as seen in Fig.2(d). However, these curves exhibit excellent symmetry both horizontally and vertically.

The total free energy F , total energy E , magnetic entropy S_M and specific heat C_M of these canonical systems can be evaluated with

$$\begin{aligned}
 F &= -k_B T \log Z_N, & E &= -\frac{\partial}{\partial \beta} \log Z_N, \\
 S_M &= \frac{E}{T} + k_B \log Z_N, & C_M &= T \left(\frac{\partial S_M}{\partial T} \right)_B,
 \end{aligned} \tag{4}$$

successively, where $\beta = 1/(k_B T)$ and Z_N is the partition function of the whole system. Figure 3(a,b) display the F , E , and C_M curves obtained with the SCA approach for the antiferromagnetic nanotube. It is very interesting to find that for the counterparting ferromagnetic tube, i.e., as $\mathcal{J}_1 = 1$ K and $\mathcal{J}_2 = 0.8$ K, the calculated F , E and C_M curves are almost exactly identical. The sudden change of E and the sharp peak in the C_M curve near T_N are the signs of phase transition.

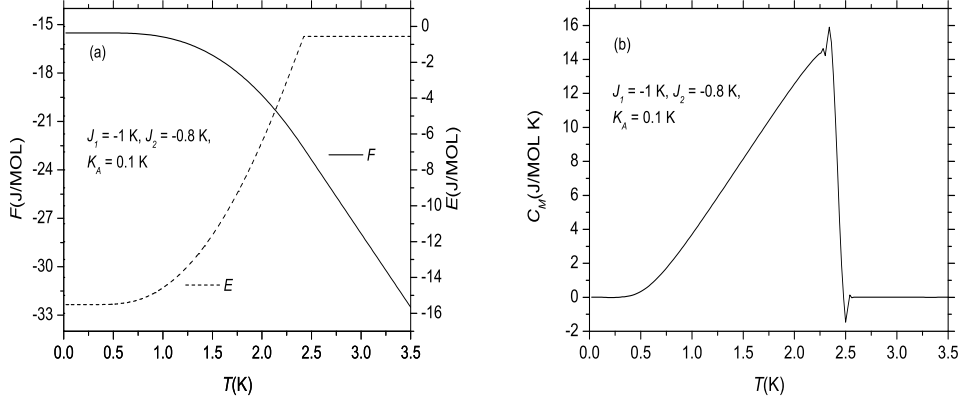


Figure 3. (a) Total energy and total free energy, and (b) specific heat, per mole of spins calculated with the SCA approach for the antiferromagnetic nanotube in the absence of external magnetic field. Here $N_L = 30$.

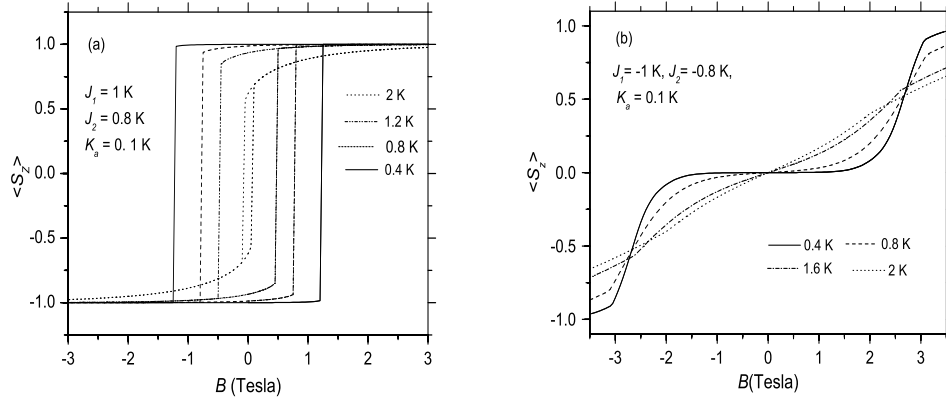


Figure 4. Hysteresis curves of the (a) ferromagnetic, and (b) antiferromagnetic nanotubes calculated with the SCA approach at different temperatures. Here $N_L = 30$.

To learn how these two sorts of nanosystems react to the external magnetic field, we then studied their hysteresis processes with the SCA approach. Fig.4(a,b) show the longitudinal hysteresis curves calculated at four different temperatures below T_M with the SCA approach for the ferromagnetic and antiferromagnetic nanotubes, respectively. In the ferromagnetic case, hysteresis loops are formed at all four temperatures. Especially at $T = 0.4$ K, the loop is almost a rectangle. If the external magnetic field is applied antiparallel to the original magnetization, all spins are suddenly rotated for 180° at $B = B_c = 1.25$ T for instance. In the antiferromagnetic case, no hysteresis loop can be formed as shown in Fig.4(b). And in the both cases, $\langle S_x \rangle$ and $\langle S_y \rangle$ always vanish if the magnetic field is exerted exactly in the z -direction. In our previous SCA simulations for an antiferromagnetic nanoparticle, it was discovered there that a strong external magnetic field, applied in the direction along which the antiferromagnetically coupled spins ordered inside the core region, could rotate them off their original direction, forming symmetric pattern around the field direction [1]. The geometrical shape of the nanotubes has indeed endowed them with very typical ferromagnetic and antiferromagnetic characters.

3 One dimensional ferromagnetic and antiferromagnetic chain models

As just described, when a weak uniaxial anisotropy along the longitudinal axis is present, all spins order spontaneously in the easy z -direction. Even when an external magnetic field is applied along the central longitudinal axis, nonzero $\langle S_x \rangle$ and $\langle S_y \rangle$ could not be observed. These peculiar features allow us to build up one dimensional ferromagnetic and antiferromagnetic chain models. In the ferromagnetic case, there are N_L equally spaced spins on the line along the longitudinal axis. The m -th spin $S_z(m)$ interacts with its left neighbor $S_z(m-1)$ and its right neighbor $S_z(m+1)$ with strength \mathcal{J}_1 , other two neighbors $S_z(m)$ on the same circle around the central axis with strength \mathcal{J}_2 . Since the spins only order in the z -direction, we then have, for the Hamiltonian given in Eq.(2), three pure eigenvectors $|\psi_1\rangle = | +1 \rangle$, $|\psi_2\rangle = | 0 \rangle$, and $|\psi_3\rangle = | -1 \rangle$ for the m -th spin, and the corresponding eigenvalues are expressed as

$$\begin{aligned}\varepsilon_1 &= -[\mathcal{J}_1 (\langle S_z(m-1) \rangle + \langle S_z(m+1) \rangle) + 2\mathcal{J}_2 \langle S_z(m) \rangle + g_S \mu_B B] - K_A, \\ \varepsilon_2 &= 0, \\ \varepsilon_3 &= [\mathcal{J}_1 (\langle S_z(m-1) \rangle + \langle S_z(m+1) \rangle) + 2\mathcal{J}_2 \langle S_z(m) \rangle + g_S \mu_B B] - K_A,\end{aligned}\quad (5)$$

respectively. This chain has a finite length N_L . However, if we let $0 \leq m \leq N_L + 1$, $\langle S_z(0) \rangle$ and $\langle S_z(N_L + 1) \rangle$ assigned to 0 at the beginning, thus all spins can be treated equally. Further assuming $\xi = \mathcal{J}_1 (\langle S_z(m-1) \rangle + \langle S_z(m+1) \rangle) + 2\mathcal{J}_2 \langle S_z(m) \rangle + g_S \mu_B B$, we finally get a formula

$$\langle S_z(m) \rangle = \frac{2 \exp(K_A/k_B T) \sinh(\xi/k_B T)}{1 + 2 \exp(K_A/k_B T) \cosh(\xi/k_B T)}, \quad (6)$$

by making use of quantum theory.

An antiferromagnet can be considered to be composed of two oppositely oriented A and B subsystems. Thus, in the simplified model, an A type spin interacts only with the nearest B -type spins, and vice versa. More specifically, an m -th A spin $S_z^A(m)$ interacts with a B -type neighbor $S_z^B(m-1)$ on its left, another B -type neighbor $S_z^B(m+1)$ on its right, both with strength \mathcal{J}_1 , and other two B type neighbors $S_z^B(m)$ belonging to the same circle around the central axis with strength \mathcal{J}_2 , and vice versa. Thus, for the same sake just described, we have once again three pure eigenvectors $|\psi_1^{A,B}\rangle = | +1 \rangle$, $|\psi_2^{A,B}\rangle = | 0 \rangle$, and $|\psi_3^{A,B}\rangle = | -1 \rangle$ for the m -th A or B spin, respectively, and the corresponding eigenvalues are given by

$$\begin{aligned}\varepsilon_1^{A,B} &= -[\mathcal{J}_1 (\langle S_z^{B,A}(m-1) \rangle + \langle S_z^{B,A}(m+1) \rangle) + 2\mathcal{J}_2 \langle S_z^{B,A}(m) \rangle + g_S \mu_B B] - K_A, \\ \varepsilon_2^{A,B} &= 0, \\ \varepsilon_3^{A,B} &= [\mathcal{J}_1 (\langle S_z^{B,A}(m-1) \rangle + \langle S_z^{B,A}(m+1) \rangle) + 2\mathcal{J}_2 \langle S_z^{B,A}(m) \rangle + g_S \mu_B B] - K_A,\end{aligned}\quad (7)$$

respectively. Assuming $\eta_{A,B} = \mathcal{J}_1 (\langle S_z^{A,B}(m-1) \rangle + \langle S_z^{A,B}(m+1) \rangle) + 2\mathcal{J}_2 \langle S_z^{A,B}(m) \rangle + g_S \mu_B B$, and making use of quantum theory, one can easily deduce a pair of coupled formulas

$$\begin{aligned}\langle S_z^A(m) \rangle &= \frac{2 \exp(K_A/k_B T) \sinh(\eta_B/k_B T)}{1 + 2 \exp(K_A/k_B T) \cosh(\eta_B/k_B T)} \\ \langle S_z^B(m) \rangle &= \frac{2 \exp(K_A/k_B T) \sinh(\eta_A/k_B T)}{1 + 2 \exp(K_A/k_B T) \cosh(\eta_A/k_B T)},\end{aligned}\quad (8)$$

for the two sorts of oppositely oriented spins.

4 Results obtained with the one dimensional magnetic chain models

Using the one-dimensional chain models, we have successfully reproduced the results given in Fig.(1,2,4), no matter if the external magnetic field was absent or applied in the z direction. There is not need to present those results here once again. Obviously, computational speed can be greatly accelerated by using these theoretical models because of their simplicity in comparison with the SCA approach.

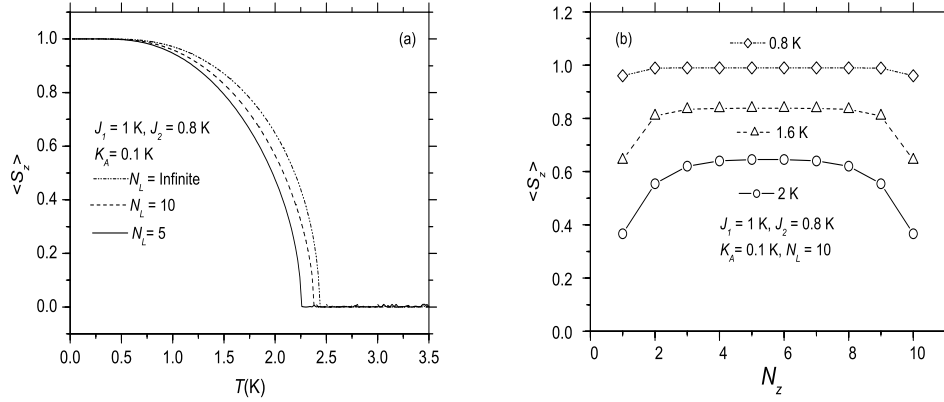


Figure 5. Calculated $\langle S_z \rangle$ (a) as the functions of temperature for the ferromagnetic nanotubes with different lengths, (b) as the functions of N_z at different temperatures for a ferromagnetic tube of length $N_L = 10$, by means of the one-dimensional ferromagnetic chain model in the absence of external magnetic field.

With the two theoretical models, it is much easy to focus our studies on the finite size effects. If the periodic condition is applied, we then have an infinitely long nanotube. Fig.5(a) depicts the spontaneous magnetization curves calculated with the one-dimensional chain model for three ferromagnetic nanotubes of finite and infinite lengths, respectively. We find here that a short tube has a low Curie temperature T_C , however the length does not strongly affect the T_C value. To fully understand the size effects, we plot the magnetization curves for the tube with a length of $N_L = 10$ at three different temperatures in Fig.5(b). Near the two ends, the spins there have weaker magnitudes than those in the middle region; and at higher temperatures, these effects become much stronger. Fig.5(b) looks very similar to Fig.1(d). But now, because of the short length, the size effects, for example at $T = 2$ K—spread deeply into the very middle part of the nanotube.

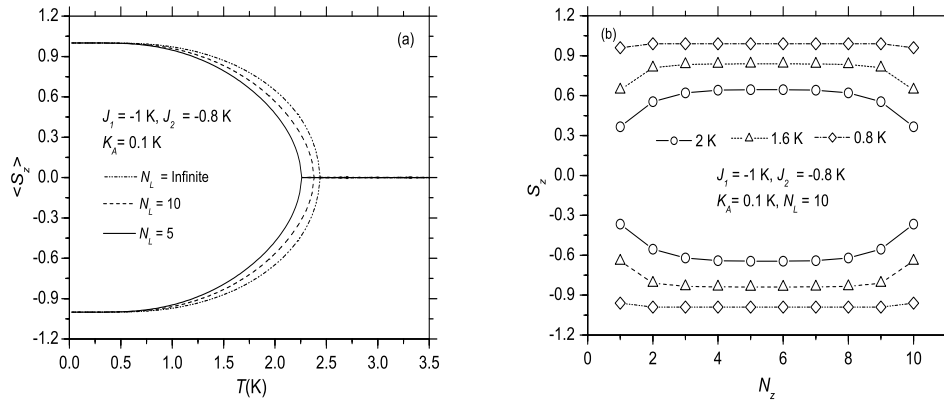


Figure 6. Calculated $\langle S_z \rangle$ (a) as the functions of temperature for the antiferromagnetic nanotubes with different lengths, (b) as the functions of N_z at different temperatures for an antiferromagnetic tube with $N_L = 10$, by means of the one-dimensional antiferromagnetic chain model in the absence of external magnetic field.

For comparison, the magnetization curves for the three antiferromagnetic tubes, as displayed in Fig.6, were calculated with the one-dimensional chain model by only changing the signs of \mathcal{J}_1 and \mathcal{J}_2 used in Fig(5) . Now we find the similar size effects as just described for the ferromagnetic nanotubes. And more interestingly, if we only draw the upper parts of Fig.6(a,b), the curves will

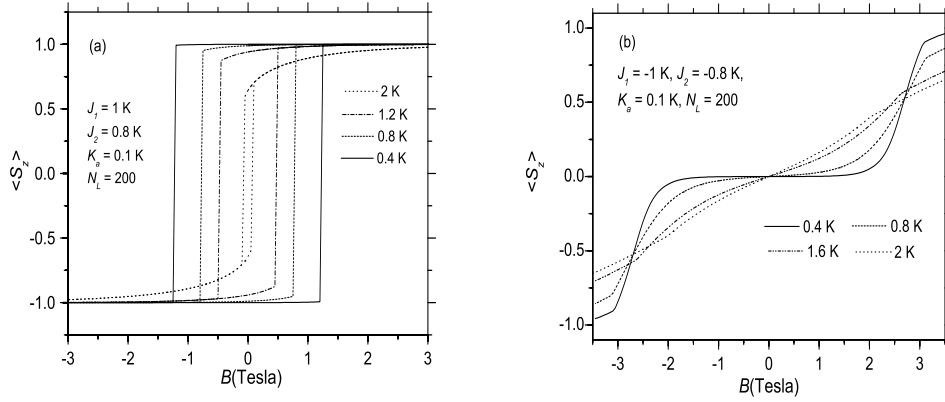


Figure 7. Calculated hysteresis curves of the (a) ferromagnetic, and (b) antiferromagnetic nanotubes at different temperatures by means of the one-dimensional ferromagnetic and antiferromagnetic chain models. Here $N_L = 200$.

coincide exactly with their counterparts depicted in Fig.5(a,b) correspondingly. Therefore, we can say the two sorts of systems are symmetric, and our calculated results are self-consistent.

The relatively faster computational speed of the theoretical models makes it easy for us to do simulations for long nanotubes. Fig.7(a,b) show the longitudinal hysteresis curves of the ferromagnetic and antiferromagnetic nanotubes of a length $N_L = 200$, obtained by means of the theoretical models using the parameters given herein. The curves shown here for the long nanotubes actually differ slightly from those shown in Fig.4(a,b), even though their lengths differ four times. Once again, the nanosystems exhibit typical ferromagnetic and antiferromagnetic characters.

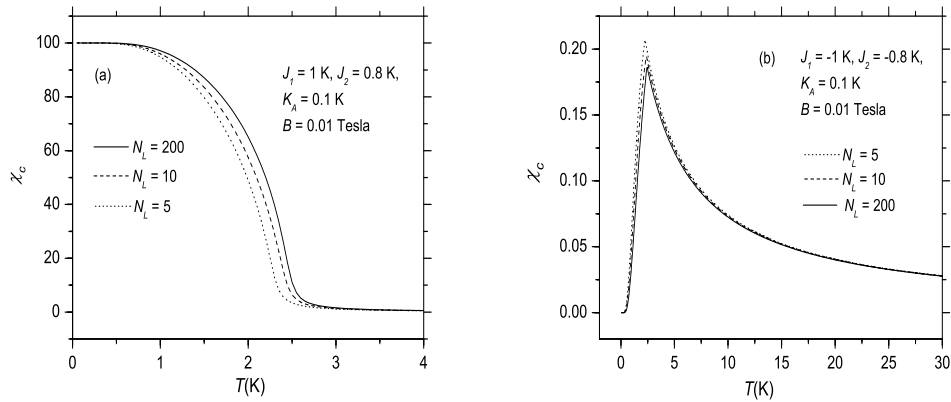


Figure 8. Calculated longitudinal susceptibility curves for (a) a ferromagnetic, and (b) an antiferromagnetic nanotubes with different lengths, by means of the one-dimensional ferromagnetic and antiferromagnetic chain models, respectively.

Finally, we calculated the susceptibilities of the two sorts of nanosystems. For the purpose, a very weak external magnetic field is usually considered to be exerted in a special direction, and the susceptibility can be approximately estimated as the ratio of the induced/enhanced magnetization to the applied magnetic field. So, we defined the longitudinal susceptibility as $\chi_c \approx \langle S_z \rangle / B$, and a field of 0.01 Tesla was assumed to be applied along the z -axis to calculate the quantities with the

one-dimensional magnetic chain models. The unit of the χ_c is 1/(Tesla Per spin). For simplicity, it is omitted in the figures.

Fig.8(a) displays the calculated results for three ferromagnetic nanotubes of different lengths. At very low temperatures, $\langle S_z \rangle$ is close to the saturated value $S = 1$, thus $\chi_c \approx \langle S_z \rangle / B \approx 100 / (\text{Tesla Per spin})$. As temperature arises, χ_c attenuates. The applied magnetic field modify each curve's shape around T_C considerably so that they attenuate continuously. Due to the size effects, we can observe here three distinct curves.

In the antiferromagnetic case, as T arises below T_N , the applied magnetic field gradually rotate those magnetic moments antiparallel to it to its direction. So in Fig.8(b), we observe that χ_c increases until T_N , where a peak appears. But above T_N , the disordering effects of temperature becomes stronger and stronger gradually, so we find all χ_c 's fade with increasing temperature. Again, we can see three curves near T_N 's, which is the evidence of size effects.

5 Conclusions and Discussion

We have also performed simulations by exchanging the magnitudes of \mathcal{J}_1 and \mathcal{J}_2 , that is, by assigning $\mathcal{J}_1 = \pm 0.8$ K and $\mathcal{J}_2 = \pm 1$ K, respectively, but we obtained the same results as those shown in Fig.(1-4). This is easy to understand. For instance, when $\mathcal{J}_1 = 0.8$ K and $\mathcal{J}_2 = 1$ K, a spin still interacts with two spins with a strength of 1 K, other two spins with a strength of 0.8 K, as in the case when $\mathcal{J}_1 = 1$ K and $\mathcal{J}_2 = 0.8$ K. So the calculated results with the two sets of parameters are naturally same.

In summary, we firstly used the SCA approach to simulate the magnetic structures for the two sorts of magnetic nanotubes, and calculated their spontaneous magnetization, longitudinal hysteresis curves and thermodynamic quantities. We found that no matter the external magnetic field was absent, or applied along the central longitudinal axis, the spins always aligned in that direction, seeming all bundled to the tubes' surface because of their peculiar geometric structure, so that the tubes exhibit typical ferromagnetic or antiferromagnetic features, which may find applications in industry. In contrast, an external magnetic field, applied in the direction along which the antiferromagnetically coupled spins align inside a nanoparticle, is able to turn the spins off the line to form symmetric pattern around the field direction [1]. Above findings in numerical simulations enable us to build up one-dimensional ferromagnetic and antiferromagnetic chain models, which could reproduce all the results obtained in SCA simulations in principle, and were then employed to investigate the size effects, and investigate the magnetic properties of long tubes. Because of the simplicity of the theoretical models, computational speed can be considerably improved. Especially, the exact agreements between our numerical calculations and theoretical analysis justify the correctness of our quantum simulation approach once again.

Acknowledgements

Z.-S. Liu acknowledges the financial support by National Natural Science Foundation of China under grant No. 11274177. H. Ian is supported by the FDCT of Macau under grant 013/2013/A1, University of Macau under grants MRG022/IH/2013/FST and MYRG2014-00052-FST, and National Natural Science Foundation of China under Grant No. 11404415.

References

- [1] Z.-S. Liu, V. Sechovsk, and M. Divi, *Physica E* 44 (2012) 826.
- [2] S. Iijima, *Nature* 56 (1991) 354.
- [3] H. Liu, D. Nishide, T. Tanaka, and H. Kataura, *Nat.Comm.* 2 (2011) 309.
- [4] H. Liu, T. Tanaka, Y. Urabe, H. Kataura, *Lett.*, 13(5) (2013) 1996.
- [5] J. A. Fagan, M. Zheng, V. Rastogi, J. R. Simpson, C. Y. Khripin, C. A. S. Batista, and A. R. H. Walker, *Nano* 7 (2013) 3373.

-
- [6] H. Liu, T. Tanaka, H. Kataura, *Nano Lett.* 14(2014) 6237.
- [7] Y. S. Lim, A. R. T Nugraha, S. J. Cho, M.Y. Noh, E.J. Yoon, H Liu, J.-H. Kim, H. Telg, E. H. Hroz, Gary D. Sanders, S.-H. Baik, H. Kataura, Stephen K. Doorn, Christopher J. Stanton, R. Saito, J. Kono, and T. Joo, *Nano Lett.* 14(3) (2014) 1426.
- [8] J.H. Gao, Q.F. Zhan, W. He, D.L. Sun, Z.H. Cheng, *Appl. Phys. Lett.* 86 (2005) 232506.
- [9] Y. Peng, T. Cullis, G. Mobus, X.J. Xu, B. Inkson, *Nanotechnology* 18 (2007) 485704.
- [10] H. N. Hu, H.Y. Chen, S.Y. Yu, *J. Magn. Magn. Matter* 299 (2006) 170.
- [11] P. Schaaf, K. Zhang, C. Lange, A. Holz, M. Weisheit, S. Fhler, *Appl. Surf. Sci.* 253 (2007) 8107.
- [12] K.M. Takata, P.T.A. Sumodjo, *Electrochim. Acta* 52(20) (2007) 6089.
- [13] L. Krusin-Elbaum, D.M. Newns, H. Zeng, V. Derycke, J.Z. Sun, R. Sandstrom: *Nature* 431 (2004) 672.
- [14] C. Gao, W. Li, H. Morimoto, Y. Nagaoka, T. Maekawa: *J. Phys. Chem. B* 110 (2006) 7213.
- [15] J. Jang, H. Yoon, *Adv. Mater.* 15 (2003) 2088.
- [16] J. Xie, L. Chen, V. K. Varadan, J. Yancey, M. Srivatsan, *Nanotechnology* 19 (2008) 105101.
- [17] I.T. Kim, R. Tannenbaum, In: Marulanda, J.M. (ed.) *Electronic Properties of Carbon Nanotubes*, pp. 33–54 (Janeza Trdine 9, 51000 Rijeka, Croatia, 2009)
- [18] J. Ding, Q. Gao, L. Xiao-Shui, W. Huang, S. Zhi-Guo, *J. Sep. Sci.* 34 (2011) 2498.
- [19] L. Bogani, C. Danieli, E. Biavardi, N. Bendiab, A.-L. Barra, E. Dalcanale, W. Wernsdorfer, A. Cornia, *Angew. Chem.* 121 (2009) 760.
- [20] H. Gul, W. Lu, P. Xu, J. Xing, J. Chen, *Nanotechnology* 21 (2010) 155101.
- [21] T. Shimada, Y. Ishii, T. Kitamura, *Phys. Rev. B* 84 (2011) 114405.
- [22] P. Landeros, O. J. Suarez, A. Cuchillo, P. Vargas, *Phys. Rev. B* 79 (2009) 024404.
- [23] B.-Z. Mi, H.-Y. Wang, Y.-S Zhou, *J. Magn. Magn. Mater.* 322 (2010) 952.
- [24] R. Masrour, L. Bahmad, M. Hamedoun, A. Benyoussef, E. K. Hlil, *State Commun.* 162 (2013) 53–56
- [25] Z.-S. Liu, V. Sechovsk, and M. Divi, *J. Phys.: Condens. Matter* 23 (2011) 016002.
- [26] Z.-S. Liu, V. Sechovsk, and M. Divi, *Phys. Status Solidi B* 249 (2012) 202.